Acta Mechatronica - International Scientific Journal about Mechatronics
Volume: 4 2019 Issue: 4 Pages: 5-10 ISSN 2453-7306

doi:10.22306/am.v4i4.50

EXPERIMENTAL VERIFICATION OF OBJECT LEVITATION BY OPTICAL SENSOR

Erik Prada
Technical University of Kosice, Faculty of Mechanical Engineering, Letna 9, Kosice, Slovak Republic, EU, erik.prada@tuke.sk (corresponding author)
Ivan Virgala
Technical University of Kosice, Faculty of Mechanical Engineering, Letna 9, Kosice, Slovak Republic, EU, ivan.virgala@tuke.sk
Martin Varga
Technical University of Kosice, Faculty of Mechanical Engineering, Letna 9, Kosice, Slovak Republic, EU, martin.varga.2@tuke.sk

Keywords: magnetic levitation; optical sensor; laser module; motion detection
Abstract: Magnetic levitation used in technical applications such as transport systems in particular high-speed trains requires position control of the levitation system. It is precisely by suitable position control that there are no hazardous situations of contact of the mechanical parts outside the magnetic cushion, which can cause a dangerous state at very high speeds. However, for correct regulation, it is necessary to first turn out a reliable position sensing subsystem. It is precisely sensing the position using the optical method that this work is devoted to. The method of shielding is verified, when a smaller collimated beam falls on the photodiode. In order to measure the changes as accurately as possible, a laser collimating beam of light was chosen as the source.

1 Introduction

Magnetic levitation has a large perspective in practice, but the widespread use of this technology is not as enormous as some other technologies. The best-known application of magnetic levitation is the use of maglev trains, but it is not the only application of magnetic levitation in practice. To meet the functional model of magnetic levitation in practice is quite problematic in our latitudes. Germany is one of the few countries dedicated to magnetic levitation technology and has a high reputation worldwide with its Transrapid train (Figure 1). However, Germany is not the only country engaged in the practical application of magnetic levitation technology. Japan has an equally strong and possibly stronger presence in this industry. While the Germans focused on one development type of Transrapid, two different types of maglevs are being constructed in Japan, working on the HSST system and the Yamanashi system. The German Transrapid train and the Japanese HSST train operate on a similar motion system of an induction linear motor, where the stationary rotor consists of an aluminium reaction pad located at the top of the track. Three-phase stator coils are placed on the lower parts of the train, creating a magnetic field. The magnetic field make train levitation and the action of the traction force induced reaction to aluminium backing gives the train moving along magnetic wave.

Incorrect positioning of the levitating train from the ground could cause a train accident in the event of unexpected events occurring during operation. For this reason, sensing the position of the levitating object is an important part for regulation needs. However, in order to design the necessary control, it is necessary to experimentally verify the position sensing by means of the optical shadow method [1-10].

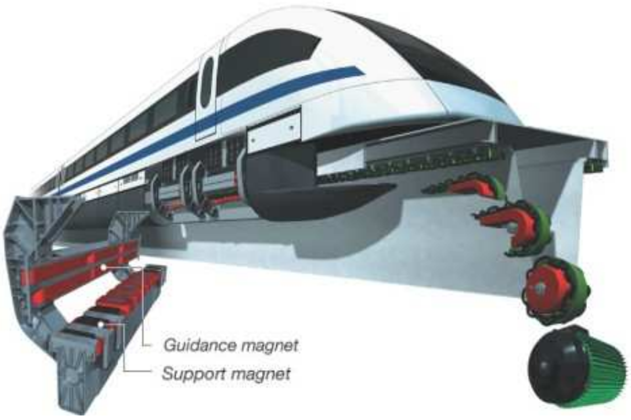

Figure 1 Transrapid train and its LIM system

1.1 Shadow method of measuring position

Magnetic levitation has a large perspective in practice, but the widespread use of this technology is not as enormous as some other technologies. The measurement of the position of the levitating object using the shadow method is based on the measurement of the current depending on the intensity of the incident light beam on the photosensitive sensor. The drop shadow on the photodiode will cause us to drop the current. Classic light or intense laser light can be used as the light beam source. The sensing unit thus consists of an emitter and an emitted beam sensor. It is most ideal to use a laser beam source as the emitter, the intensity of which is better reflected in the photodiode in a way of greater variance of the measured values. The figure (Figure 2) shows a diagram of the construction of the sensing. When designing it is appropriate to use a collimator, which provides us collimated beam.

The figure description:
1. coil
2. levitating object
3. photodiode
4. laser module with collimator
5. collimated laser beam

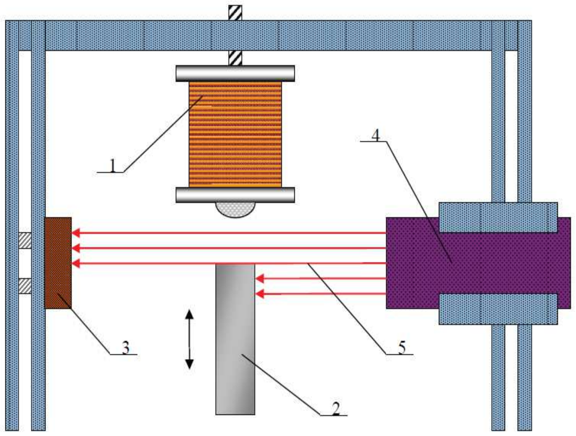

Figure 2 Schematic representation of the position sensing solution by the shadow method [2]

2 Experimental verification of the shadow method

The absolute measurement method was used for experimental verification. The aim of the measurement was experimental verification of the proposed solution. The experiment was performed under different conditions and settings and was therefore divided into several phases. The determined dependency characteristic is therefore different for each phase.

In the experiment we used LASER BTL 2000, LED light and Tesla 1PP75 photodiode. The BTL 2000 laser is primarily intended for medical use. Its positive feature is the great variability of possible settings. Negative can be considered the divergence of the radiated beam, whose angle was 36˚. The active surface of the Tesla 1PP75 photodiode is 3.5 mm x 5.5 mm.

Current measurement was performed on a HP 34401A professional laboratory multimeter. The experiment was carried out on a rack set, on which the Laser BTL 2000 probe was mounted and compared to the photodiode Tesla 1PP75. The casting of the shadow on the photodiode was obtained using a metal sheet that was mounted in a rack with micrometres movement in the X-axis and Y-axis directions. Schematic representation of the measurement is in the figure (Figure 3).

Description of measurement scheme:
1. Laser module holder
2. Laser module
3. photodiode
4. Stand with micrometre movement
5. Metal shielding plate
6. photodiode holder
7. ammeter

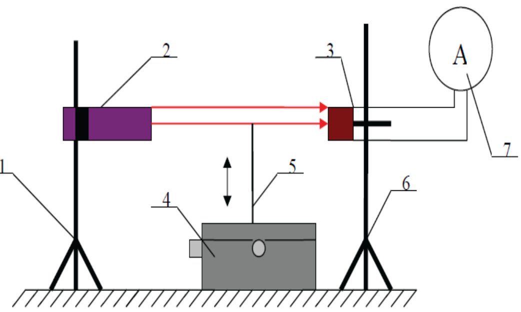

Figure 3 Scheme of current measurement by laser beam on photodiode [2]

Measurement procedure:
- connecting the laser to the mains, attaching the laser probe to the stand and connecting the photodiode through the wires to the multimeter input,
- turning on the laser and checking the beam so that it hits the sensor,
- setting the distance of the sensor from the laser module as required,
- grasping the shielding plate in a micrometres feed rack,
- zero setting of the shielding plate,
- turning on the multimeter and setting the DC current mode,
- recording the generated background currents of the measuring room,
- reading the value from the multimeter with zero cover,
- turn the screw to change the position of the shielding plate in 0.5 mm increments until the entire 10 mm interval has passed.
- reading three values from the multimeter every half millimetre and writing to the table,
- calculation of averages from the measured values and subsequent correction for total measurement error,
- Interpolation graphs [4].

Experimental verification consisted of three phases of measurement when the laser beam conditions changed [4].

For experimental phase I, we determined the following measurement conditions:
- Daylight measurements,
- continuous laser beam,
- laser beam power 8 mW,
- distance of probe from photodiode 100 mm.

For experimental phase II we determined the following measurement conditions:

- Daylight measurements,
- 990 Hz pulsed laser beam,
- laser beam power 8 mW,
- distance of probe from photodiode 100 mm.

For experimental phase III, we determined the following measurement conditions:

- Daylight measurements,
- 500 Hz pulsed laser beam,
- laser beam power 8 mW,
- distance of probe from photodiode 100 mm.

3 Results of measuring position

The measured values were averaged and then corrected for the measurement error using the formula (2). The correction of the measured values (Table 1) consisted of subtracting the measurement error from the averaged value. We used the formula (1) to calculate the measurement error.

$$\delta_i = \delta_{REi} + \delta_{RAi} = [(0{,}01\% \times I_{xi}) + (0{,}004\% \times 100)] \quad (1)$$

$$Ix_{KOR\,i} = Ix_i - \delta_i \quad (2)$$

3.1 Results of experimental phase I

The calculated values of the corrected current (Table 1) of the first experimental phase were shown as polynomial dependence in the (Figure 4), described by formulas (3), (4).

Table 1 Errors and correct values of the phase I - measurement process [4]

	1.	2.	3.	4.
δ_i [mA]	0,01104	0,01094	0,01092	0,01078
IxKOR [mA]	70,39	69,39	69,19	67,79
	5.	6.	7.	8.
δ_i [mA]	0,00948	0,00814	0,00678	0,00567
IxKOR [mA]	54,79	41,39	27,79	16,69
	9.	10.	11.	12.
δ_i [mA]	0,00432	0,00412	0,0041	0,0041
IxKOR [mA]	3,12	1,19	0,99	0,99
	13.	14.	15.	16.
δ_i [mA]	0,00408	0,00408	0,00407	0,00407
IxKOR [mA]	0,79	0,79	0,69	0,69
	17.	18.	19.	20.
δ_i [mA]	0,00406	0,00407	0,00407	0,00407
IxKOR [mA]	0,59	0,69	0,69	0,69

$$y = 0{,}0023x^6 - 0{,}0459x^5 + 0{,}1115x^4 + 2{,}9304x^3 - 19{,}928x^2 + 20{,}255x + 68{,}064 \quad (3)$$

$$R^2 = 0{,}9928 \quad (4)$$

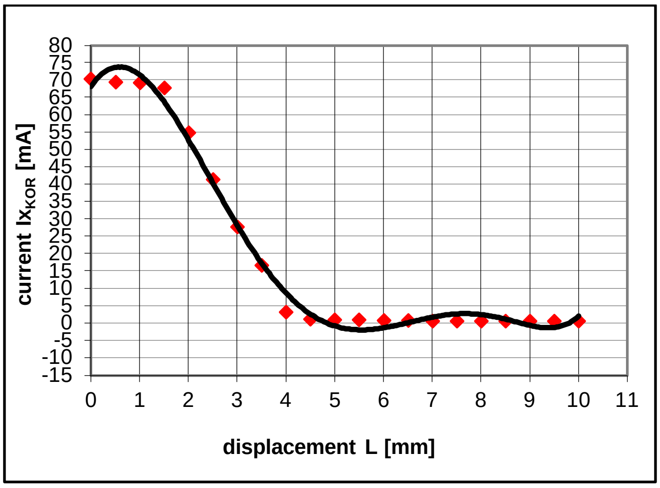

Figure 4 Graph of interpolation of corrected current versus cover length – phase I [2]

Since in our case we are mainly interested in the linear course of the graph because of the correct positioning and then the subsequent coil regulation, we focus mainly on the values forming the most linear parts of the graph. The shape of the graph is in the (Figure 5) and the interpolation equation is attached.

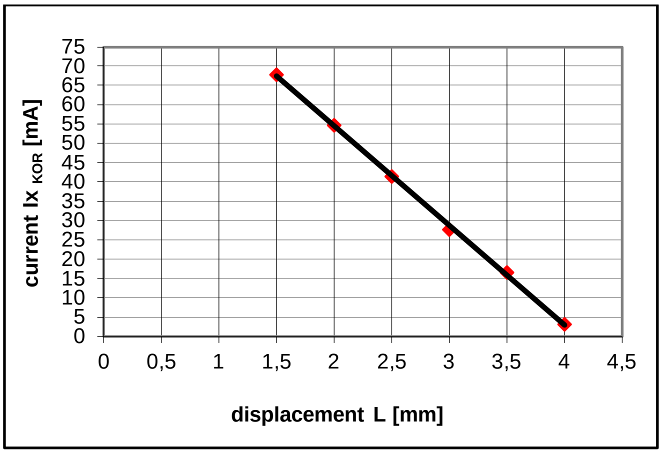

Figure 5 Graph of linear interpolation of selected work area values of phase I [2]

$$y = -25{,}786x + 106{,}17 \quad (5)$$

$$R^2 = 0{,}999 \quad (6)$$

3.2 Results of experimental phase II

The calculated values of the corrected current (Table 2) of the second experimental phase were shown as the polynomial dependence in the (Figure 6), described by formulas (7), (8).

Volume: 4 2019 Issue: 4 Pages: 5-10 ISSN 2453-7306

Table 2 Errors and correct values of the phase II - measurement process [4]

	1.	**2.**	**3.**	**4.**
δ_i [mA]	0,00869	0,00871	0,00881	0,00875
IxKOR [mA]	46,89	47,09	48,09	47,49
	5.	**6.**	**7.**	**8.**
δ_i [mA]	0,00875	0,00872	0,00820	0,00729
IxKOR [mA]	47,49	47,19	41,99	32,89
	9.	**10.**	**11.**	**12.**
δ_i [mA]	0,00628	0,00535	0,00449	0,00418
IxKOR [mA]	22,79	13,49	4,89	1,79
	13.	**14.**	**15.**	**16.**
δ_i [mA]	0,00419	0,00414	0,00413	0,00412
IxKOR [mA]	1,89	1,39	1,29	1,19
	17.	**18.**	**19.**	**20.**
δ_i [mA]	0,00412	0,00412	0,00412	0,00411
IxKOR [mA]	1,19	1,19	1,19	1,09

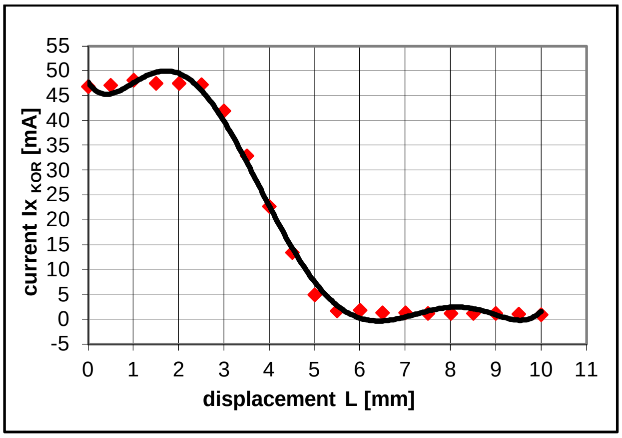

Figure 6 Graph of interpolation of corrected current versus cover length – phase II [2]

$$y = 0{,}0065x^6 - 0{,}2038x^5 + 2{,}3622x^4 - 11{,}953x^3 + 23{,}275x^2 - 13{,}702x + 47{,}685 \quad (7)$$

$$R^2 = 0{,}9955 \quad (8)$$

In the second experimental phase we were also interested in the linear part of the graph, because of the correct positioning and then the coil regulation. The shape of the graph is in the figure (Figure 7). It can be seen that the values obtained from the pulsed laser are almost completely linear and therefore this linearity can also be used for positioning. During this phase, the linear character values start at 2 mm and end at 5.5 mm.

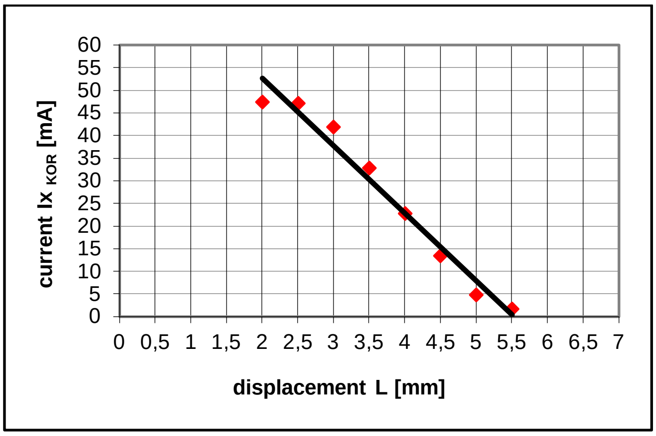

Figure 7 Graph of linear interpolation of selected work area values of phase II [2]

$$y = -14{,}929x + 82{,}547 \quad (9)$$

$$R^2 = 0{,}971 \quad (10)$$

3.3 Results of experimental phase III

The calculated values of the corrected current (Table 3) of the experimental phase III were shown as the polynomial dependence in the (Figure 8), described by formulas (11), (12).

Table 3 Errors and correct values of the phase III - measurement process [4]

	1.	**2.**	**3.**	**4.**
δ_i [mA]	0,00953	0,00938	0,00927	0,00834
IxKOR [mA]	55,29	53,79	52,69	43,39
	5.	**6.**	**7.**	**8.**
δ_i [mA]	0,00683	0,00609	0,00548	0,00433
IxKOR [mA]	28,29	20,89	14,79	3,29
	9.	**10.**	**11.**	**12.**
δ_i [mA]	0,00415	0,00412	0,00411	0,00411
IxKOR [mA]	1,49	1,19	1,09	1,09
	13.	**14.**	**15.**	**16.**
δ_i [mA]	0,0041	0,00412	0,00415	0,0041
IxKOR [mA]	0,99	1,19	1,49	0,99
	17.	**18.**	**19.**	**20.**
δ_i [mA]	0,0041	0,0041	0,00412	0,00411
IxKOR [mA]	0,99	0,99	1,19	1,09

The shape of the linear waveform is shown in the figure (Figure 9). It can be seen from the graph that the values obtained from the pulse laser at 500 Hz are decreasing faster to zero and differ more from linearity than at a higher frequency.

EXPERIMENTAL VERIFICATION OF OBJECT LEVITATION BY OPTICAL SENSOR
Erik Prada; Ivan Virgala; Martin Varga

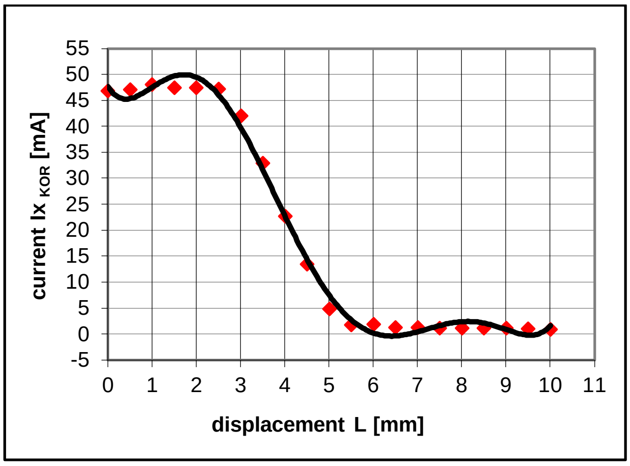

Figure 8 Graph of interpolation of corrected current versus cover length – phase III [2]

$$y = -0{,}0024x^6 + 0{,}0918x^5 - 1{,}3532x^4 + 9{,}4181x^3 - 28{,}958x^2 + 17{,}816x + 54{,}157 \quad (11)$$

$$R^2 = 0{,}9949 \quad (12)$$

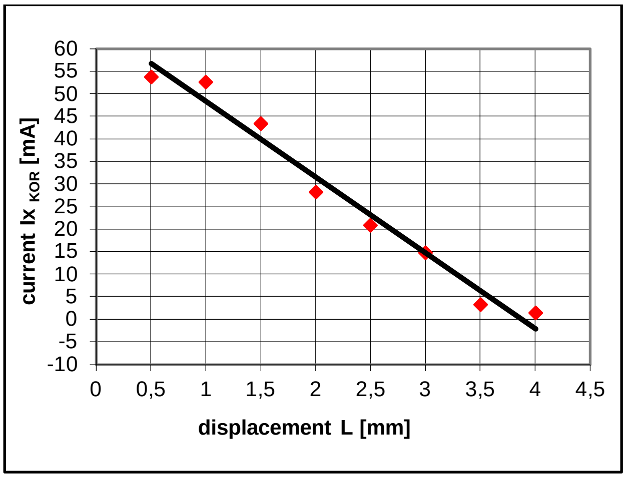

Figure 9 Graph of linear interpolation of selected work area values of phase III [2]

$$y = -16{,}817x + 65{,}165 \quad (13)$$

$$R^2 = 0{,}9747 \quad (14)$$

Conclusions

From the experimental verification of the shadow method for the purpose of determining the position of the levitating object and for the subsequent need for regulation, we found that the dependencies of the corrected values of the individual phases of measurement differ slightly from each other. For the purpose of positioning we are interested mainly in the linear course of the corrected values depending on the displacement of the object [11-12].

Acknowledgement
The authors would like to thank to Slovak Grant Agency – project KEGA 018TUKE-4/2018 "Implementation of new technologies and educational methods in the field of control systems to improve education level and practical skills of graduates of Mechatronics" and project VEGA 1/0389/18, "Research and development of kinematic redundant mechanisms".

References

[1] REICH, Š.: *Design of functional model of magnetic levitation*, Diploma thesis, Kosice, TU-SjF, 2003. (Original in Slovak)
[2] PRADA, E.: *Contactless sensor for positioning of levitating object*, Final thesis, Kosice, TU-SjF, 2009. (Original in Slovak)
[3] GMITERKO, A., KELEMEN, M., DOVICA, M., CAPÁK, M.: *Miniature mobile robot for moving in a tube with small diameter*, Proceedings of the 2nd International Conference Mechatronics and Robotics '99, Brno, Czech Republic, pp. 67-70, 1999.
[4] KELEMEN, M., GMITERKO, A., GÓTS, I.: Mechatronic concept of bristled in-pipe machine, *ATP Plus*, Vol. 2001, pp. 48-52, 2001.
[5] VITKO, A., JURIŠICA, L., BABINEC, A., DUCHOŇ, F., KĽÚČIK, M.: *Some Didactic Problems of Teaching Robotics*, Proceedings of the 1st International Conference Robotics in Education 2010, Bratislava, Slovak University of Technology in Bratislava, pp. 27-30, pp. 67-70, 2010.
[6] HAVLÍK, Š., HRICKO, J., PRADA, E., JEZNÝ, J.: *Linear motion mechanisms for fine position adjustment of heavy weight platforms*, TUKE, 2020.
[7] VIRGALA, I., KELEMEN, M., PRADA, E., LIPTÁK, T.: Positioning of Pneumatic Actuator Using Open-Loop System, *Applied Mechanics and Materials*, Vol. 816, pp. 160-164, 2015.
[8] LIPTÁK, T., DUCHOŇ, F., KELEMENOVÁ, T., PUŠKÁR, M., KELEMEN, M., KURYŁO, P., PRADA, E.: Analysis of Uncertainty of Tilt Measurement with Accelerometer, *Applied Mechanics and Materials*, Vol. 611, pp. 548-556, 2014.
[9] PRADA, E., BALOČKOVÁ, L., VALÁŠEK, M.: Elimination of the Collision States of the Effectors of Industrial Robots by Application of Neural Networks, *Applied Mechanics and Materials*, Vol. 798, pp. 276-281, 2015.
[10] PRADA, E., VALÁŠEK, M., GMITERKO, A.: Simulation and Determination of the Influence of the Gait Function on the Change of the Shape of a Snake-Like Robot, *Applied Mechanics and Materials*, Vol. 789-790, pp. 636-642, 2015.
[11] SPANIKOVA, G., SPANIK, P., FRIVALDSKY, M., PAVELEK, M., BASSETTO, F., VINDIGNI, V.: Electric model of liver tissue for investigation of

electrosurgical impacts, *Electrical Engineering*, Vol. 99, pp. 1185-1194, 2017.

[12] KONIAR, D., HARGAS, L., SIMONOVA, A., HRIANKA, M., LONCOVÁ, Z.: *Virtual Instrumentation for Visual Inspection in Mechatronic Applications*, 6th Conference on Modelling of Mechanical and Mechatronic Systems (MMaMS) Location: High Tatras, SLOVAKIA, pp. 227-234, 2014.

Review process

Single-blind peer review process.